Temperature control on deep tectonic tremor belt in the Nankai subduction zone

Ryoya Ikuta[1], Yui Kobayashi[2], Riko Arai[1], Tatsuhiko Kawamoto[1]

1. Department of Geosciences, Faculty of Science, Shizuoka University, Shizuoka, 422-8529 Japan
2. Shizuoka-Higashi Highschool, Shizuoka, Japan

Key Points:

- Revelated fluid from oceanic crust beneath non-convective mantle wedge causes the deep tectonic tremors.
- Ise gap of the deep tectonic tremor belt is explained as the locations where the hanging wall is not mantle wedge but crust.
- Kii gap of the deep tectonic tremor belt is not a gap in the direction orthogonal to the plate convergence.

Abstract

Deep tectonic tremors occur in the Nankai subduction zone, defining a belt-like zone with a width of a few ten km located at depths between 30 and 55 km along upper surface of the subducting Philippine sea slab. We interpret the geometry of the tremor belt based on temperature calculations. Time evolution of temperature is calculated using a 3-D heat conduction assuming constant geometry of the slab and the present-day plate convergence velocity. The results show that the tremors occur along the 450°C isotherm along the slab surface where the mantle wedge can be non-convective and already well-serpentinized. Two gaps of the tremor belts are explained by different mechanisms. The Ise gap is where the hanging wall is not mantle wedge but crust. The Kii Gap is not a gap orthogonal to the plate convergence direction, but only appears to be a gap because the isotherm of the plate surface steps in the plate convergence direction. The tremors can be caused by high pore-fluid pressure conditions due to aqueous fluids released by dehydration reactions in blueschist-facies oceanic crust to form eclogite facies. The depth of the tremor belt corresponds to that of decoupled, non-convective mantle wedge. Since the temperature and pressure are within the serpentinite stable condition, the released fluid would normally be absorbed by serpentinization of the mantle wedge peridotite. However, since the non-convective mantle wedge is already well serpentinized from exposure to previously released fluids, the newly released fluid is not absorbed and increases the pore pressure.

Plain Language Summary

Deep tectonic tremors in the Nankai trough form belt-like zone on the plate boundary only to a specific along-strike extent with two blank areas in the zone. These tremors are thought to be caused by fluid released from the subducting slab, which raises pore pressure. We discuss their occurrence condition based on

temperature calculation, shape and motion of the slab. The results suggest that the fluid is released from the slab only once under certain temperature and that the tremors occur at the location. The temperature condition is that the fluid is released from the oceanic crust and at the same time the mantle absorbs more fluid. For pore pressure to increase in such a location, the mantle must already be saturated. This is consistent with the idea that the tip of mantle wedge does not flow but rather decouples from the subducting slab. The tremors form the belt only in specific regions where the released fluid contacts with the decoupled mantle wedge. An absence of tremors at the contact with the continental crust also suggests that the presence of minerals such as antigorite may also be a key for the tremors.

1. Introduction

Deep tectonic tremor (Obara, 2002) and long-term slow slip (Hirose et al., 1999) were first reported in the Nankai subduction zone, where the Philippine sea plate (PHS) is subducting beneath the Amur plate (AM), and subsequent studies have documented slow earthquake phenomena beneath many trenches worldwide (see the review by Obara, 2020). These slow earthquakes occur in a frequency band different from normal earthquakes and are governed by a different scaling law (Ide et al., 2007). The small amplitudes of the seismic waves generated by these events indicate the low frictional strength of the source fault, which is most likely to be related to high pore pressure (e.g., Julien, 2002; Obara, 2002), which is consistent with the results of seismic tomography (Shelly et al., 2006; Nakajima & Hasegawa, 2016).

Episodic tremor and slip (ETS) in the Nankai, Cascadia (e.g., Rogers & Dragert, 2003), and Mexico (Husker et al., 2012) subduction zones defines a "tremor belt" along the down-dip edge of the coupling zone of megathrust earthquakes. We interpret the geometry of the tremor belt based on 3-D temperature calculations. We focus on two features of the tremor belt in the Nankai subduction zone (Figure 1; Nakajima et al. 2007; Annoura et al., 2018): (1) the depth of ETS varies regionally from 30 to 55 km, assuming that the ETS occurs on the slab surface (e.g., Hirose et al., 2008; Shiomi et al., 2008); and (2) ETS does not occur beneath Ise Bay (Figure 1, B) or the Kii Channel (Figure 1, D). We discuss these features with reference to the geometry of the slab surface, the velocity vector of plate convergence, and temperature profiles and provide constraints on the cause of the ETSs. Hereafter we use the term 'tremor' rather than 'ETS' because we do not consider the slip.

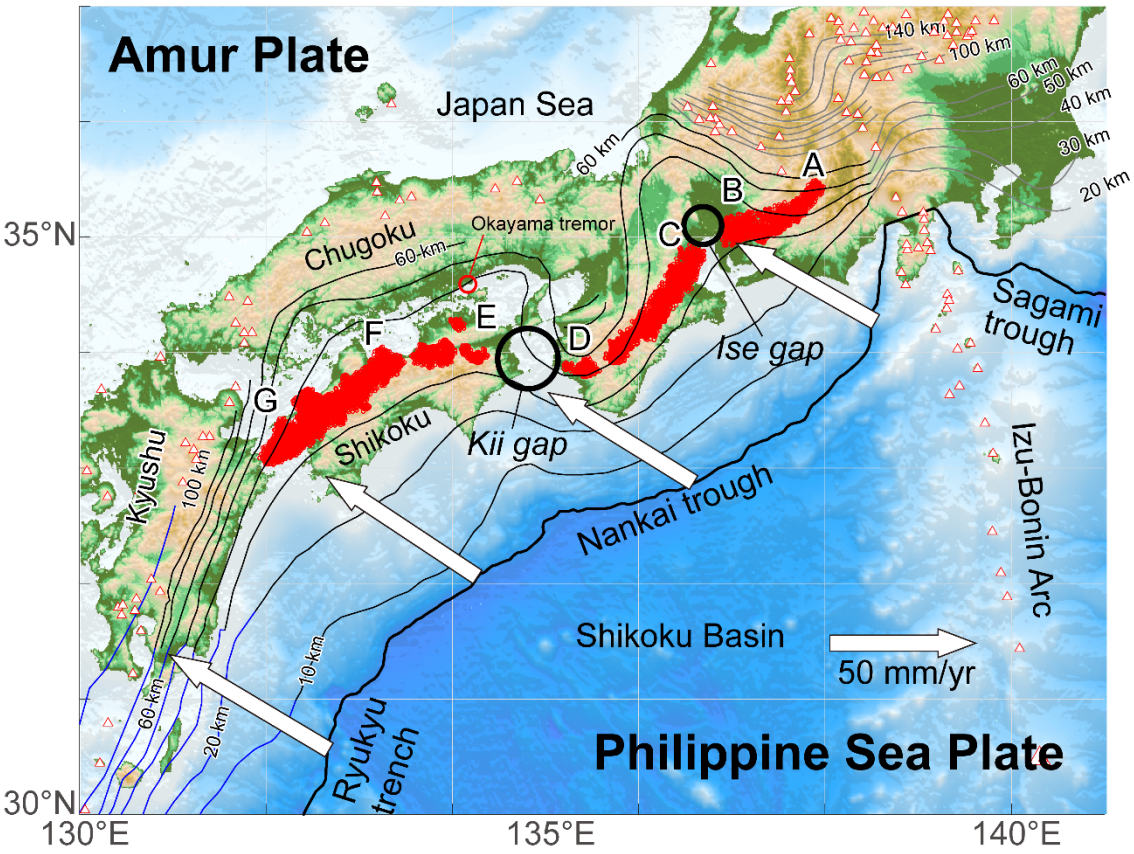

Figure 1. Tectonic setting and location of the tremor belt in southwestern Japan. The Philippine sea plate (PHS) is subducting beneath the Amur plate (AM) along the Nankai trough and the Ryukyu trench. White arrows show plate velocity of PHS relative to AM by DeMets et al. (2010). Contours indicate the depth of the slab surface at intervals of 10 km. Black, gray, and blue contours indicate data from Nakajima et al. (2007), Hirose et al. (2008), and Tatsumi et al. (2020), respectively. Red dots indicate tremor epicenters determined by Annoura et al. (2016). Triangles represent Quaternary volcanoes (Global Volcanism Program, 2014). The black circles indicate the Ise and Kii gaps in the tremor belt. Letters indicating locations along the tremor belt correspond to those in Figure 2a. The small red circle to the north of the letter "E" indicates the focal region of the Okayama tremor (Ide & Tanaka, 2014).

1. **Subducting slab model**

Here we compare models of the subducting slab and select the model that best accounts for the depth of the tremor hypocenters in the Nankai trough. Various slab-surface models have been proposed (e.g., Baba et al., 2002; Hirose et al., 2008; Shiomi et al., 2008; Ide et al., 2010; Hayes, 2018). The models differ

because of differences in data coverage and a priori information. The depth of the tremor belt on the slab surface differs among the models (Figure 2a). Nevertheless, in all models except the low-resolution Slab 2.0 model, the depth of the tremor belt deepens eastward of the Ise gap (B to A, Figure 2a), deepens westward between the Ise and Kii gaps (C to D), and deepens westward of the Kii gap (E to G). Low-frequency earthquakes (LFEs) occur at the same locations as the tremors, and their hypocenters have been determined by Kato & Nakagawa (2020) from the arrival times of S-waves. The LFEs show an along-trough trend similar to that of the tremors. Figure 2b shows the deviation of the tremor depths from the hypocenter depths of the LFEs determined by Kato & Nakagawa (2020), averaged every 0.1 ± 0.1° in longitude. Among the five models, Nakajima et al. (2007) model has the smallest east–west variation in depth difference across the Kii gap (Figure 2b). The temperature model of the slab was calculated using the slab-surface model of Nakajima et al. (2007). Other slab-surface models are described in the Supplementary Information.

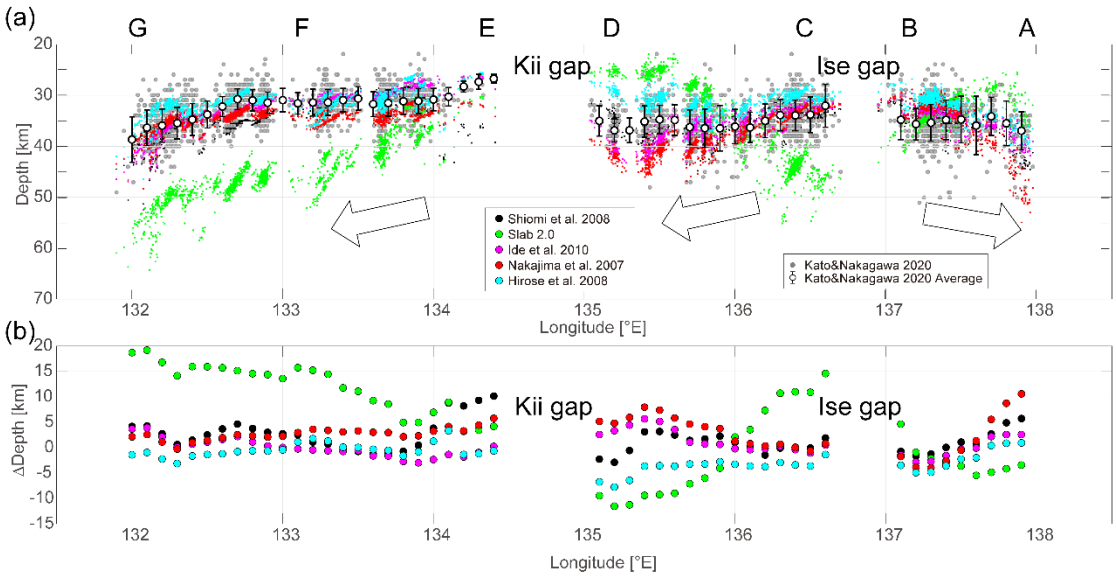

Figure 2. (a) Depths of the slab surfaces from the slab models of Shiomi et al. (2008; black dots), Slab 2.0 (Hayes 2018; green dots), Ide et al. (2010; pink dots), Nakajima et al. (2007; red dots), and Hirose et al. (2008; cyan dots) at the epicenter locations of the LFEs. 5 km is subtracted from the oceanic Moho surface model of Shiomi et al. (2008). Gray dots represent the hypocenter depths of LFEs from Kato & Nakagawa (2020) using S-wave arrivals, and open circles with error bars represent their averaged depths over ±0.1° in longitude. Locations indicated by letters A–G at top correspond to those in Figures 1 and 4. (b) Deviation of the averaged slab surface depths (±0.1° in longitude) from the hypocenter depths (open circles in (a)) of Kato & Nakagawa (2020). Symbol colors are as in (a).

1. **Calculating the temperature of the subducting slab**

A 3-D heat conduction and advection model is used to calculate the temperature field of the subducting PHS slab. The finite difference method is used for the calculation, employing the following conditions: (1) heat moves only by 3-D conduction and slab subduction, as convection in the mantle wedge is not included; (2) the slab is a medium with constant thickness that subducts along its present-day surface profile at the present-day rate of plate convergence; and (3) the initial temperature field is given by a one-dimensional semi-infinite cooling model. The consideration of convection in the mantle wedge is likely to yield higher temperatures than those obtained using the conduction model, and will be considered if the absolute temperature estimates are considered to be important.

3-1. Model geometry and equations

The 3-D model is composed of a rectangular solid with dimensions of 11.6° in longitude (up to ~1,100 km), 9.5° in latitude (up to ~1,000 km), and 170 km depth, within which 1,453,701 regular grid points are set at 0.05° intervals in the east–west and north–south directions, 2 km intervals in the vertical from the surface to 50 km depth, 5 km intervals in the vertical from 50 to 100 km depth, and 10 km intervals in the vertical at depths greater than 100 km. The equations of heat conduction are solved for these grid points and the time evolution of temperature is calculated with the finite difference method. The other grid points are set along the slab geometry (Figure 3) at spatial intervals corresponding to a subduction time of 50,000 years (i.e., 0–4 km) in the direction of plate convergence and 5–10 km in the direction orthogonal to convergence, and a constant interval of 2 km in the direction normal to the slab surface. The grid points in the slab are used only for calculating the temperature distribution within the slab during subduction, which represents heat advection due to the downward movement of the slab. Heat conduction is calculated using only the regular grid points (i.e., those grids consisting the rectangular solid), employing the temperature distribution updated by movement of the slab and interpolation from the slab grid points to the regular grid points. To clearly show the contrast in temperature distribution within and outside the slab due to this shift related to downward movement of the slab, an extra 10 km thickness of no-shift grid points (i.e., 4 layers of grid points) is set above and below the slab (black grid points in Fig. 3b). The initial temperature structure of the regular grid points is given by a semi-infinite cooling model as follows:

$$T(z,t) = (T_m - T_0) erf(\tfrac{z}{2\sqrt{\mathrm{t}}}) + T_0, \quad (1)$$

$$\kappa = \tfrac{k}{\rho c_p} \ ,$$

where z is depth, T_0 is the Earth surface temperature, T_m is the initial temperature of the asthenosphere, k is the thermal conductivity, is the density of the medium, and c_p is the specific heat of the medium at constant pressure. These parameters are assumed to be common in the mantle and crust for simplicity

(Table 1). The time t of the initial state is assumed to be 15 Myr before the present, coinciding with the cessation of spreading in the Shikoku basin.

For the one-dimensional initial condition, the temperature shift in the slab grid results in an inhomogeneous 3-D temperature distribution. From this distribution, the temporal evolution of temperature is calculated by the following heat diffusion equation:

$$\frac{\partial T}{\partial t} = \kappa \nabla^2 T. \quad (2)$$

In each cycle of the calculation, we first solve equation (2) for the regular grid points to calculate the temporal evolution of temperature by conduction over a period of 50,000 years, and then pass the new temperature to the slab grid and shift the grid by one grid point in the direction of subduction to represent heat advection due to subduction over the same time period. This cycle of conduction calculation and temperature shift is repeated until the end of the 15 Myr period of the experiment.

The shape of the subducting PHS slab is from Nakajima et al. (2007). The motion of the PHS has varied throughout its subduction history. According to Isezaki (1986), the Japan Sea basin continued to spread until about 15 Ma, as southwestern Japan rotated clockwise. This coincided with ENE–WSW spreading in the Shikoku basin, which started at ~26 Ma and ended at ~15 Ma (Okino et al. 1994). The history of magmatic activity in southwestern Japan suggests that subduction of the PHS stopped during the period of spreading in the Shikoku basin, and resumed at ~6 Ma (Kimura et al. 2014). We ignore the different cooling histories of the central and marginal parts of the Shikoku basin and the movement of the PHS prior to the cessation of subduction. We assume that the Shikoku basin, which was in a cooling phase during the 15 Myr from 21 Ma, began subducting at 6 Ma at the same rate as that of the present day. The vector of subduction for each location is computed using the Euler pole and the rotation velocity of the PHS relative to the AM (54.8°N, 160.6°E; 1.126 deg Myr^{-1} clockwise; DeMets et al., 2010).

The temporal evolution of temperature from 6 Ma to the present is calculated using the above geometry, motion, and initial temperature distribution of the slab. It is assumed that there is no heat transfer through the sides or bottom of the 3-D model; i.e., $\frac{\partial^2 T}{\partial x^2} = 0$ (x is the direction normal to the model boundary). In terms of advection, the slab always subducts at the trench and does not enter or leave through the boundaries of the model. For areas at depth in the model where the presence of the slab is not certain, it is assumed that no slab exists, and the slab is set to disappear when it subducts beyond the point.

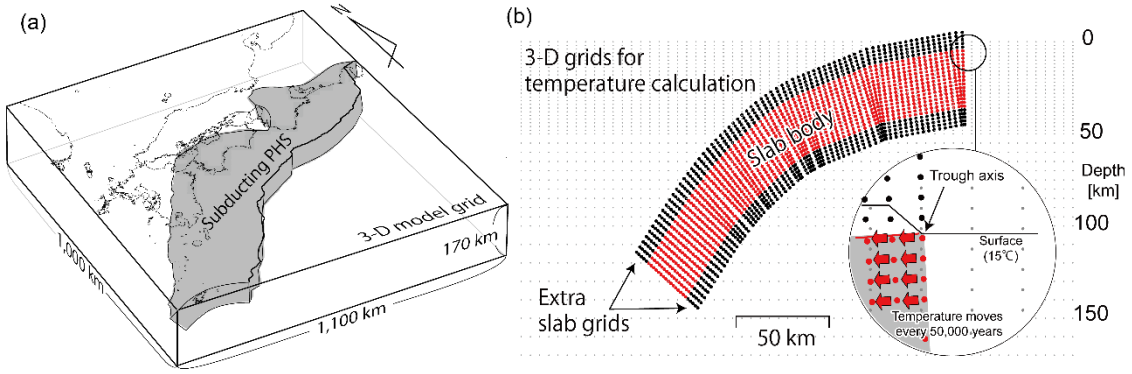

Figure 3. A 3-D model used for temperature calculation. (a) Slab configuration in the calculation field. Gray volume indicates the slab body of the subducting PHS. The solid curve along up-dip edge of PHS indicates the Nankai trough. (b) Vertical cross-section through the 3-D model, oriented parallel to the direction of subduction. Gray dots indicate the regular grid points used to calculate thermal conduction. Red solid circles indicate grid points within the subducting slab. The slab grid points are used to move the temperature field in the direction of subduction at each time step, every 50,000 years (inset). The solid black circles above and below the slab body represent extra grid points that are added to ensure the accurate projection of the temperature distribution near the slab boundaries onto the regular (conduction) grid points.

Table 1. Parameters for temperature calculation

Parameter	Name	Value
c_p [J kg^{-1} K^{-1}]	Isobaric specific heat	1.046×10^3 †
[kg/m^3]	Density of the mantle	3.4×10^3
T_m [℃]	Initial asthenosphere temperature	1350 ‡
T_0 [℃]	Surface temperature	15
k [W m^{-1} K^{-1}]	Thermal conductivity	4.184 †

†From Hamaguchi et al. (1983).

‡From Takenaka et al. (1999).

1. **Result**

Figure 4 shows the temperature of the slab surface at 6 Myr after the start of subduction. Shallow extensions of the hot zone at the eastern and western ends of the slab are due to an edge effect of the slab grid model. The temperature distribution at sites located >50 km from the slab ends, which are not affected by edge effects, shows that at a given depth the slab temperature is higher in areas with a smaller angle of subduction than in areas with a higher angle of subduction. This pattern arises because it takes longer for a slab with a lower

angle of subduction to reach a given depth. Figure 5 shows the temperature distribution in vertical cross-sections along the direction of plate convergence. The shape of the isotherms varies with the subduction angle of the slab.

Tremors are assumed to occur on the slab surface. The depth of hypocenters varies systematically along the strike of the slab from 30 to 55 km, whereas the isotherms fall within the range of 400–500°C regardless of location (Figures 4 and 5). Figure 6a shows depth or temperature versus distance from the Euler pole between PHS and AM (DeMets et al. 2010). The temperature is more constant than the depth, except in the region between points E and F.

The Kii gap spans up to 1° in longitude on the map but only 0.2° in Figure 6a in the direction normal to the slab motion. In addition, the cluster near point E in Figure 1 appears to be the second zone on the back-arc side of the main tremor belt in the eastern Shikoku fills the Kii gap if we consider the direction of slab motion (Figure 4). In other words, the tremor clusters align in a direction orthogonal to the direction of slab motion.

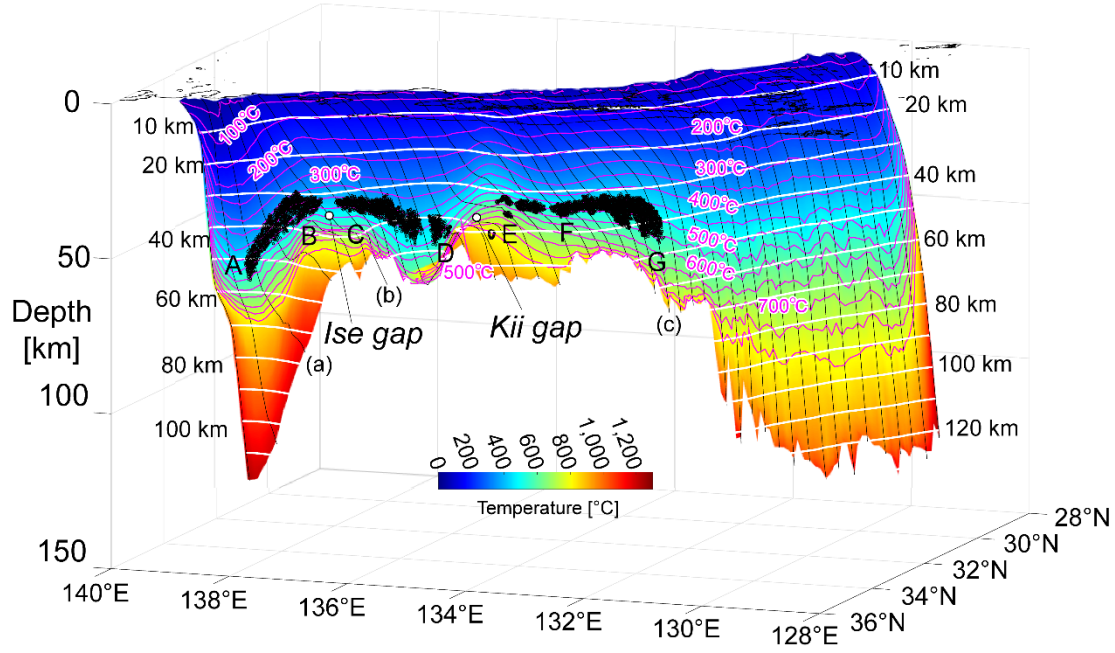

Figure 4. Calculated temperature (color scale) on the slab surface at 6 Myr after the initiation of subduction, viewed overhead from the NNW. The slab-surface model is from Nakajima et al. (2007). Pink lines are isotherms with an interval of 50 °C. White lines on the slab surface are isodepth contours with an interval of 10 km. The epicenter of tremors (Annoura et al. 2016) are projected on the slab surface as black dots. The tremor belt is oblique to the isodepth contours. Black vertical lines on the slab surface are projections of small circles

that indicate the plate motion direction, based on DeMets et al. (2010). The points along the tremor belt indicated by letters A–G correspond to those in Figures 1 and 2, and the small circles indicated by (a)–(c) correspond to the cross-sections in Figure 5.

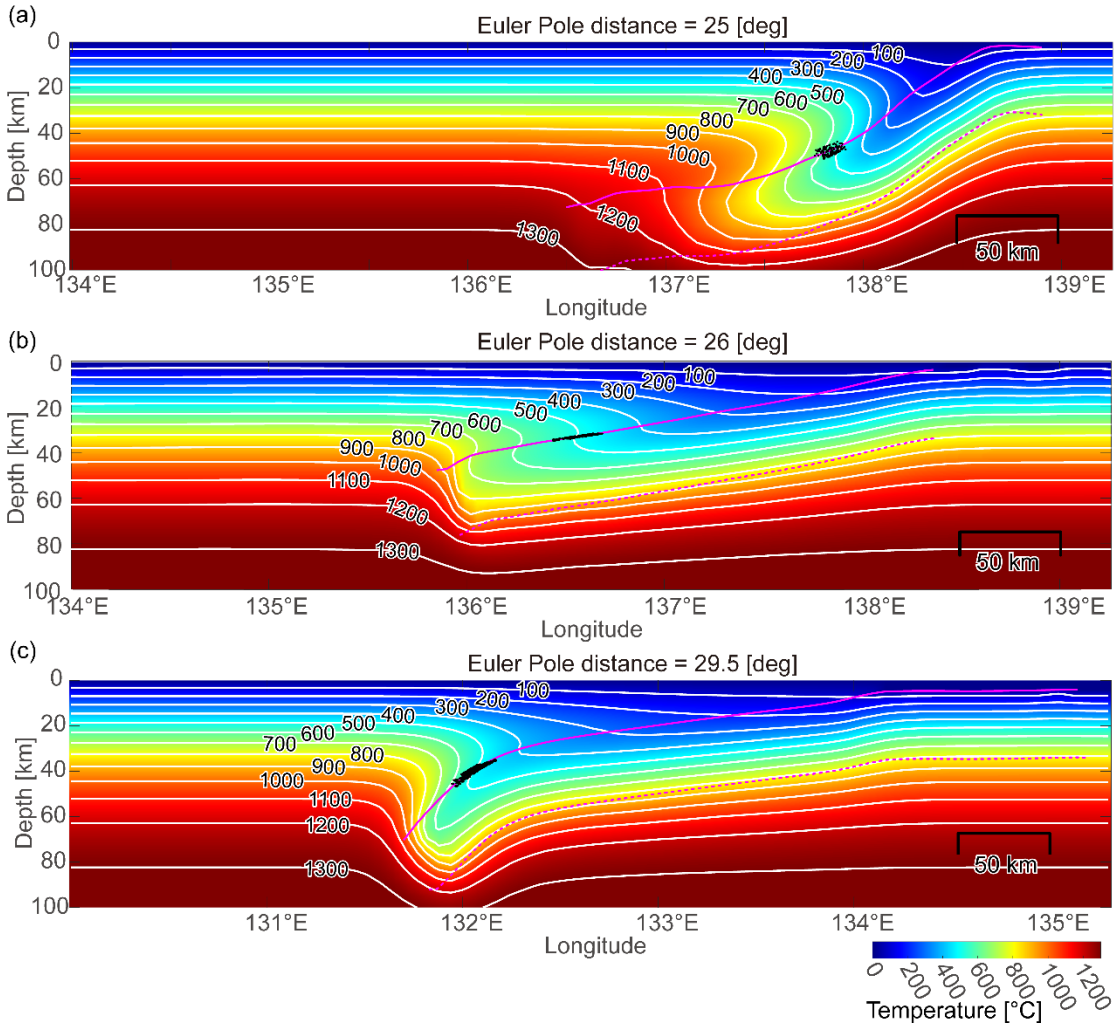

Figure 5. Cross-sections of the thermal structure beneath the Nankai trough along small circles at 25° (line "a" in Figure 4), (b) 26° (line "b" in Figure 4), and (c) 29.5° (line "c" in Figure 4) from the Euler pole. White contours indicate isotherms with an interval of 100°C. Solid and dotted pink lines indicate the upper surface and base of the subducting slab, respectively.

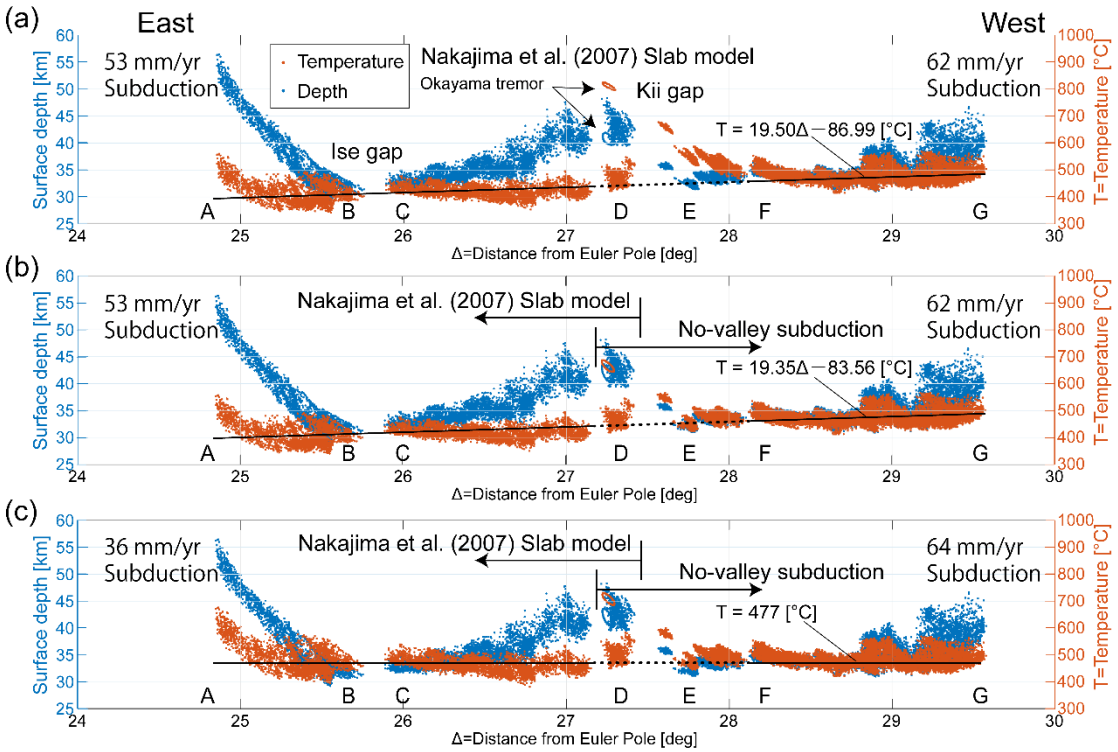

Figure 6. Depth and temperature of the slab upper surface in the region beneath the tremor epicenters. The x-axis represents the distance from the Euler pole between the PHS and the AM. The temperature and depth are equally scaled by the averaged standard deviation each 0.1°. The straight black line is the least squares approximation of the temperature using the formula T = 19.50Δ – 86.99, except for x-axis distances of 27.2–28.1° (dashed line). (a) Temperature is calculated based on the slab model of Nakajima et al. (2007) and velocity data of DeMets et al. (2010). (b) Temperature calculated based on Nakajima et al. (2007) model to the east of the Kii gap (location E) and based on no-valley subduction model for the area of Okayama tremor and to the west of the Kii gap (Figure S1). (c) Temperature is calculated by tripling the deviation of the subduction rate of the PHS from the average value over the entire length of the trough.

1. Discussion

5-1. Fluid supply from downgoing oceanic crust

The locations of tremor epicenters are not concordant with the isodepth contours of the slab surface of subducting PHS; instead, they are sub-parallel to the 450 °C isotherm. The thermal structure of the subducting oceanic lithosphere controls the along-dip location of tremor. This indicates that tremors

are caused by aqueous fluids resulting from dehydration reactions in the oceanic lithosphere, with the reactions being controlled by temperature rather than pressure. The temperature of 450°C leads to dehydration reactions related to (1) a transition from the blueschist facies to the eclogite facies in oceanic crust, and (2) a transition from antigorite + brucite to forsterite + H_2O in oceanic mantle (Figure 7; Maruyama et al. 1986; Evans 2004). The former transition is expected to release much more aqueous fluid than the latter, as the amount of aqueous fluid released in the latter is related to the amount of brucite, which typically occurs in minor amounts. The close relations between temperature of the downgoing oceanic crust and the locations of tremors has been pointed out by the previous studies (Yoshioka et al., 2008). Yoshioka et al. (2008) introduced the dehydration rate which can be important to control the density of tremors. It is important to suggest the H_2O dehydrated from the downgoing oceanic slab to the mantle peridotite to make antigorite, a high-pressure form of serpentine until fully serpentinized mantle wedge, at least at the base of the wedge. Aqueous fluids can be present in such fully serpentinized mantle, which results in lowering normal stress to cause tremors.

Hydrous minerals in subducting oceanic crust are dehydrated at 450 °C to deliver aqueous fluids towards the plate boundary and the base of the mantle wedge. Such fluids lead to the serpentinization of mantle wedge peridotite under temperature of 450–600℃ (Figure 7). In this temperature range, un-serpentinized mantle wedge can absorb the fluids, resulting in a reduction in pore pressure. In contrast, serpentinized mantle wedge cannot accommodate more fluid, resulting in an increase in pore pressure. The tremors occur under such conditions at the base of the well-serpentinized mantle wedge above the locations of slab dehydration.

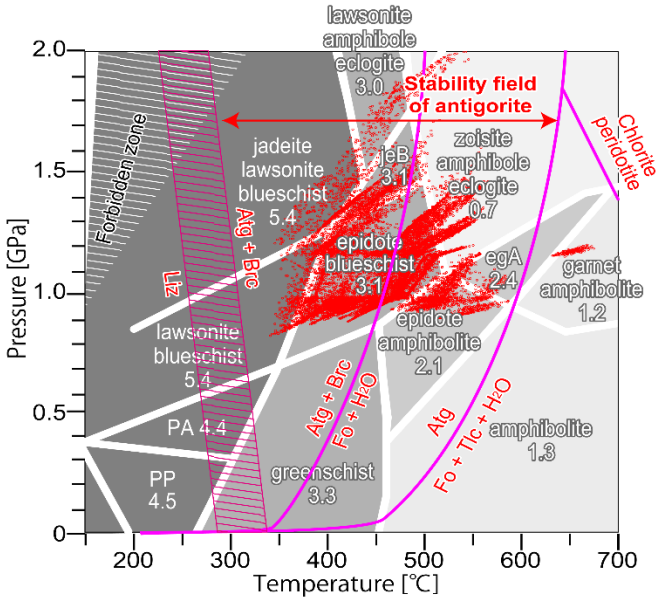

Figure 7. Calculated temperatures of the slab surface at location of the tremor hypocenters superposed on metamorphic facies fields (gray lines; modified from Maruyama et al., 1996) and the phase diagram for serpentine (pink lines; Evans 2004). Dots indicate the temperature and pressure of the slab surface at the locations of tremor epicenters (see Figure 6a). Abbreviations of facies names: BS = blueschist; Zeo = zeolite; PP = prehnite–pumpellyite; PrA = prehnite–actinolite; PA = pumpellyite–actinolite; GS = greenschist; AP = actinolite–calcic plagioclase; EA = albite epidote amphibolite; AM = amphibolite; HGR = high-pressure granulite; GR = granulite; Am EC = amphibole-eclogite subfacies. Abbreviations of serpentine mineral names: Liz = lizardite; Atg = antigorite; Brc = Brucite; Fo = forsterite; Tlc = talc.

5-2. Subducting slab model

The tremors west of the Kii gap (in the region between E and F in Figure 6a) are inconsistent with the overall temperature dependence of tremor activity in the studied section of the Nankai trough. We examine the calculation model with regard to this inconsistency, and further discuss a model in which a tear exists in the slab at around the location of the Kii gap. Next, we investigate the effect of the subduction rate on the overall temperature increase from east to west.

The calculated high temperatures at shallow depths in the E–F region might have arisen because the slab that subducted from the southern tip of Kii peninsula (near to D) was once heated at depth and then returned to shallower levels assuming slab motion along present-day shape of the slab surface. However, such a depth history for the slab surface may be unrealistic. It is more likely

that once a slab sinks, it does not return to shallower levels. However, to introduce temporal variation in the shape of the slab surface, we must adopt other assumptions that are poorly constrained, such as the deformation history and mantle rheology.

As a second-best model, we conduct separate calculations for the periods before and after a change in the shape of the slab. We calculate the temperature of the shallow slab to the west of the Kii gap as if the slab had arrived at its present location by sliding along a slab surface without valley, which is done by filling the valley in the original model (Figure S1). Then we combine this result for the western side of the Kii gap with that for the eastern side, as calculated using the present-day slab geometry.

The new temperature distribution at the tremor epicenters is flatter along the trough (Figure 6b). The unusual high temperature in the E–F region shown in Figure 6a disappears in Figure 6b (Figure S2). Given the relationship between tremor and temperature, it seems more likely that the shallow slab in the eastern part of the Shikoku near area E (Figure 6b) was subducted to this location while maintaining its shallow depth.

The boundary between the eastern part of the original model and the western part of the new model is the northern extension of the Kinan seamount chain, along which there possibly exists a tear in the PHS slab, as inferred from microearthquake distributions and receiver function analysis (Figure S1; Ide et al. 2010). This tear in the slab was also proposed by Cummins et al. (2002) based on the seismic structure. The existence of a tear is also indicated by earthquake clusters triggered by subsurface fluids (Yoshida et al, 2011) and mantle-derived hot springs with high $^{3}He/^{4}He$ ratios (Wakita et al. 1987; Sano & Nakajima 2007). The other slab models, including those of Nakajima et al. (2007), Hirose et al. (2008), and Shiomi et al. (2006), show a curve in the slab around the area of the seamount chain, but not a tear. The differences in slab depth among these models (Figures 1, S3, and S4) indicate that the depth of the upper surface of the slab is poorly constrained in this area. It is also difficult to conclude whether the slab is torn or just bending sharply, if considering only the link between temperature and tremors.

Following the concept of spherical-shell tectonics proposed by Yamaoka et al. (1986), we estimate the excess or deficiency in area of the upper surface of the subducted slab by assuming that the surface retains its pre-subduction area on the spherical shell. The distance measured along the slab surface, orthogonally from the meridian of 139°E, is compared with the distance on the spherical shell along the surface. If we assume a tear in the area of the extension of the Kinan seamount chain, the spherical shell is ~20 km less in maximum width than the bending slab modeled by Nakajima et al. (2007), suggesting a gap in the slab in this region. The calculation is not based on the model of Nakajima et al. (2007) itself, but on a slab model in which the deeper part below 70 km is extrapolated (see Figure 8) to maintain continuity of the slab surface. In conclusion, the torn slab model is supported from the perspective of spherical-shell tectonics, too.

Although there is small deficit in area at a depth of 30 km around the tremor belt and the area of missing slab is ~100 km farther north, the torn slab enough causes steep temperature and pressure offset which would cause offset of the tremor belt.

Judging from the cross-sections along various latitudes, the width of the area without slab, as inferred from spherical-shell tectonics, is generally narrower than the width of the aseismic area without intra-slab earthquakes (Figure S5). Here the slab depth to the east of the tear, which has not been identified from observation, is extrapolated for the area computation. The slab in this area may have been bent downward by slab pull and/or slab anchor force (i.e., resistance by the mantle wedge) to further widen the area without slab, and the eastern end of the slab on the western side of the tear might be shallower than in the no-tear model. On the western side of the tear, there is an offset in the temperature distribution between the tremor clusters (vertical arrows in Figure 6a), which may be due to the normal or transform fault structures near the spreading axis that create a rupture as the slab is torn and pulled apart.

In this study, we focus only on the tremor catalog of Annoura et al. (2016), but some tremor activity is not included in this catalog; e.g., a cluster named 'Okayama tremor' (Ide & Tanaka 2014) occurs near area E (Figure 1). The approximate extent of this cluster is shown by an ellipse in Figures 1, 4, and 6. The slab surface beneath the epicenter of the Okayama tremor is about 40 km, which coincides with the reported hypocenter depth by Ide & Tanaka (2014) that best explains the seismic waveform. The Okayama tremor appears to overlap with the tremor belt on the forearc side in the direction of plate motion across the tear. The positional overlap may be an apparent result of locally different movements of the torn slab, but even so, it remains uncertain why the clusters in region E and the Okayama tremor do not appear to follow a continuous isothermal line and why they are isolated from the tremor belt.

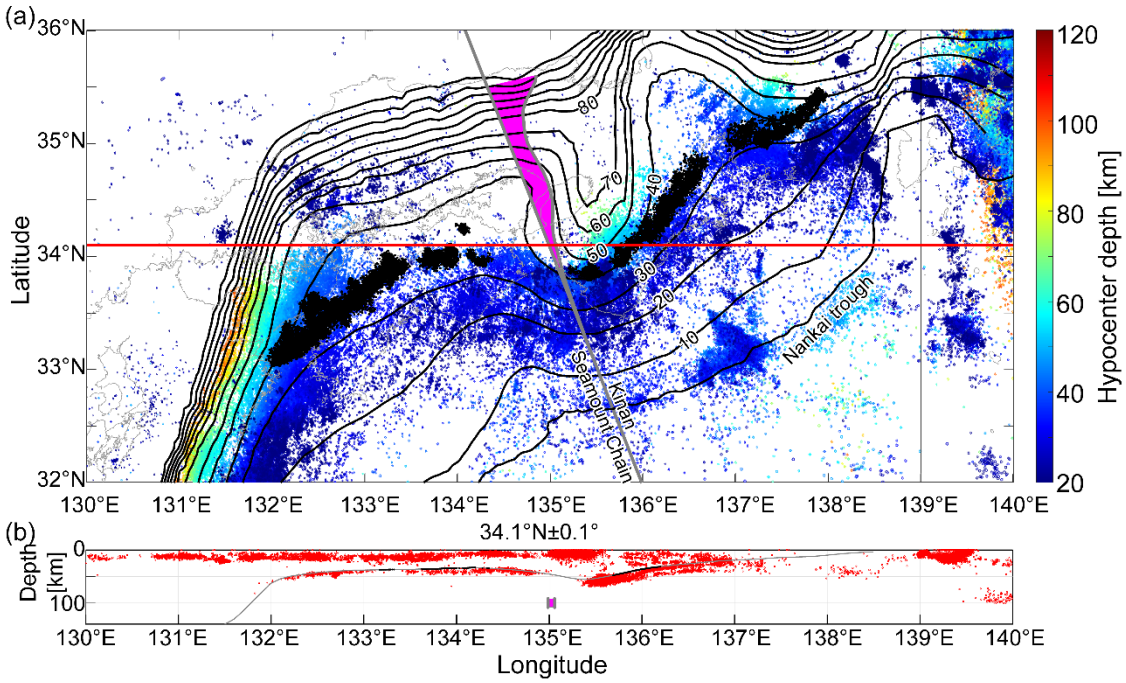

Figure 8. Deficit in slab width predicted by spherical tectonics. (a) Map view of the area of slab deficit (pink shading) assuming a slab tear along the northern extension of the Kinan seamount chain. Dots indicate earthquakes hypocenters at depths of 20–120 km, as detected by the Japan Meteorological Agency (JMA) from January 2000 to December 2020; the dots are color-coded according to depth. Black dots indicate the epicenters of the tremors. (b) Cross-section along 34.1°N latitude, as indicated by the red line in (a). Red dots indicate the earthquakes hypocenters within 10 km from the 34.1°N latitude. Thin black curve shows the upper surface of the subducting slab. Black dots on the curve shows the hypocenter of the tremor whose depth is fixed on the slab surface.

The temperature of the slab surface tends to become higher towards the west (Figure 6b). Excluding the E–F region, the linear fitting of the first model calculation shows an increase in temperature towards the west with a slope of 18.38 K/deg against longitude (Figure 6a). If slab dehydration occurs via a specific reaction at a certain temperature and pressure, this temperature trend could accompany systematic change of the slab surface depth. However, there is no east–west trend in tremor depth (Figure 2). If so, the temperature trend could be an apparent phenomenon due to calculation. The temperature of the slab surface is controlled by the subduction velocity, with a lower (higher) temperature being associated with a faster (slower) subduction velocity. In the current subduction model of DeMets et al. (2010), the subduction velocity is 52 and 71 mm/yr at the eastern (35°N, 139°E) and western (28°N, 130°E) ends

of the trench on the slab grid, respectively. We vary this subduction velocity linearly along trough without changing the average value of 61.5 mm/yr to eliminate the along-trough temperature gradient. The new model increased the along-trough velocity gradient by a factor of three compared to the old one. The new subduction velocity is 34 and 89 mm/yr at the eastern and western ends of the modeled trough, respectively. The resulting temperature profile shows no trend along the trough (Figure 6c). The new velocity at the eastern end of the tremor belt is 36 mm/yr, which is similar to the actual value of 42 mm/yr reported by Nishimura et al. (2007) based on a local geodetic model. The convergence rate of 89 mm/yr along the Ryukyu trench at the western end of the model is also within a reasonable range, considering the trench retreat caused by back-arc opening along the Ryukyu Arc and the resulting subsidence of the slab. Ultimately, the linear east–west trend in temperature in our original model would be within the range of variation among different subduction models.

Figure 9a shows the temperature distribution calculated using the modified model with the no-valley subduction and the larger velocity gradient which corresponds to Figure 6c. Figure 9b shows the P–T conditions at the points on the slab where tremors occur. The tremors are concentrated around the boundary between the blueschist and amphibole-eclogite facies, which suggests that dehydration reactions in the crustal rock liberate fluids that migrate into the mantle wedge and create favorable conditions for tremor on the slab surface.

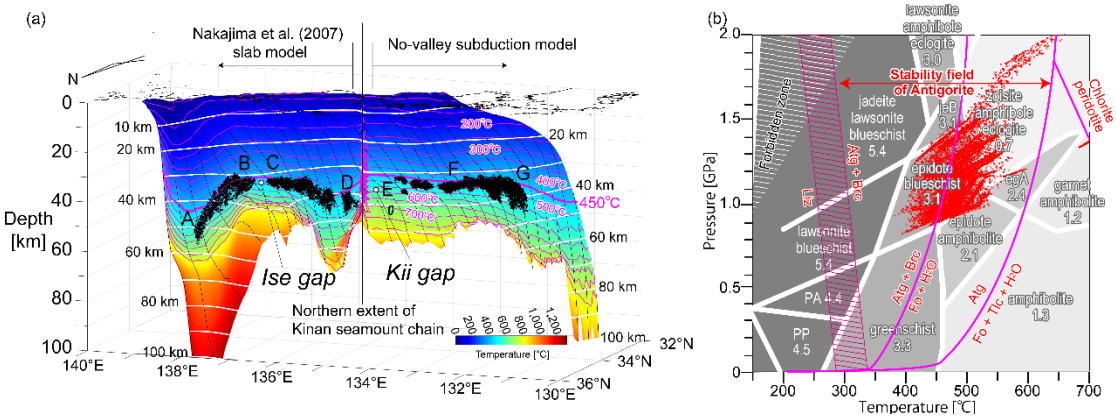

Figure 9. Temperature distribution calculated using the modified model with the no-valley slab surface and the tripled subduction velocity gradient, which corresponds to Figure 6c. (a) Same as Figure 4, but using the modified model. (b) Calculated temperatures superposed on metamorphic facies fields and the phase diagram for serpentine. Dots indicate the temperature and pressure of the slab surface at tremor epicenters, based on Figure 6c.

5-3. Gaps in the tremor belt, and the ends of the belt

Tremors do not occur in the Ise gap (Figure 4). Iidaka et al. (2017) reported that the subducted slab beneath this region is in direct contact with continental

crust, as inferred from receiver functions and seismic wave velocity tomography. In contrast, the tremor zones would be located within the mantle wedge. In the western part of the tremor belt, the thickness of the continental crust from Kii peninsula to Shikoku is ~30 km, as inferred from seismic reflection data (Salah & Zhao 2004) and receiver functions (Shiomi et al. 2006), whereas the slab surface along the tremor belt is located at depths of >30 km (Figure 4). This suggests that the tremors are occurring when the hanging wall is composed of mantle rock, as noted by Shelly et al. (2006) and Shiomi et al. (2004). Nakajima & Hasegawa (2016) undertook a seismic tomography study and reported that around the Ise and Kii gaps, the hanging wall at 3 km above the slab surface has lower V_P, lower V_P/V_S, and higher attenuation than the surrounding area, indicating a high metamorphic grade and low pore pressure; i.e., the plate boundary is well drained. Aqueous fluids might originate from the slab beneath the Ise gap; however, the conditions in the hanging wall act to suppress the occurrence of tremor.

Suenaga et al. (2018) proposed that little fluid is liberated from the slab in the Ise gap. These authors performed 2D temperature calculations based on observed heat flows around the gap and calculated dehydration gradients (wt%/km) in crustal rock along the direction of subduction. Their results indicate that weaker dehydration is expected in the Ise gap than in surrounding areas. However, since their dehydration gradient is an average over a range of 3–5 times the width of the tremor zones, the dehydration gradients are not fairly evaluated. Our calculations yield a steep temperature gradient (K/km) around the Ise gap, which is comparable with that in surrounding areas. Aqueous fluid is being produced beneath Ise gap but does not result in pore pressure enhancement.

The blank area of the tremor belt beneath the Kii channel, orthogonal to the direction of subduction, is not as wide as it appears in map view (Figures 4 and 6). The tremor belt is almost continuous in a direction orthogonal to the slab motion direction, indicating that the fluid stored in the slab is definitely liberated to generate the tremors. Whether the remaining sliver of the gap without tremor contacts with continental crust as well as in the Ise gap or not remains unclear due to the uncertainty in the estimated depth of the slab around the tear.

The isotherms on the slab surface become deeper outside of the eastern and western ends of the tremor belt due to the high angle of subduction (Figure 4; note that in the figure the isotherms at the eastern end of the tremor belt returns to a shallower depth due to the apparent effect of the edge of the slab). Wada et al. (2008) numerically simulated the rheology of a mantle wedge and showed that the slab surface shallower than 70–80 km is decoupled from the mantle wedge due to a weak interface layer composed of talc. In a study of the Shikoku region in the Nankai trough, Wada & Wang (2009) proposed that the downdip limit of decoupling is 60 km. This suggests that the tip of the mantle wedge is well-serpentinized by continued exposure to the slab dehydration-derived fluids

over long periods of time due to lack of convection. On the other hand, in the deeper part of a mantle wedge, interplate coupling generates mantle wedge convection, which brings un-serpentinized peridotite from back-arc side toward the slab surface, where it absorbs fluid and effectively reduces inter-plate pore pressure (Figure 10). This indicates that tremor occurs along plate boundaries overlain by serpentinized mantle, which is formed by the dehydration of oceanic crust through eclogite formation under conditions of 450°C and 1–2 GPa. Such conditions occur in relatively hot subduction zones such as those at the Nankai and Cascadia (e.g. Behr & Burgmann, 2021).

Regarding the Cascadia subduction zone, the deep tremor belt is distributed at a similar depth to that in the Nankai Trough but the temperature may be slightly higher. Ji et al. (2017) calculated the slab surface temperature at about 700℃ in the tremor belt in the Cascadia, which is much hotter than that in the Nankai subduction zone in this study and others (e.g. Yoshioka & Murakami, 2007). However, their calculated temperature is unrealistically high at 300°C at the trench axis, suggesting that overall temperature is over-estimated. It is open to study the slab surface temperature and the depth range of the non-convective mantle wedge for Cascadia and other subduction zones where deep tremor belts exist.

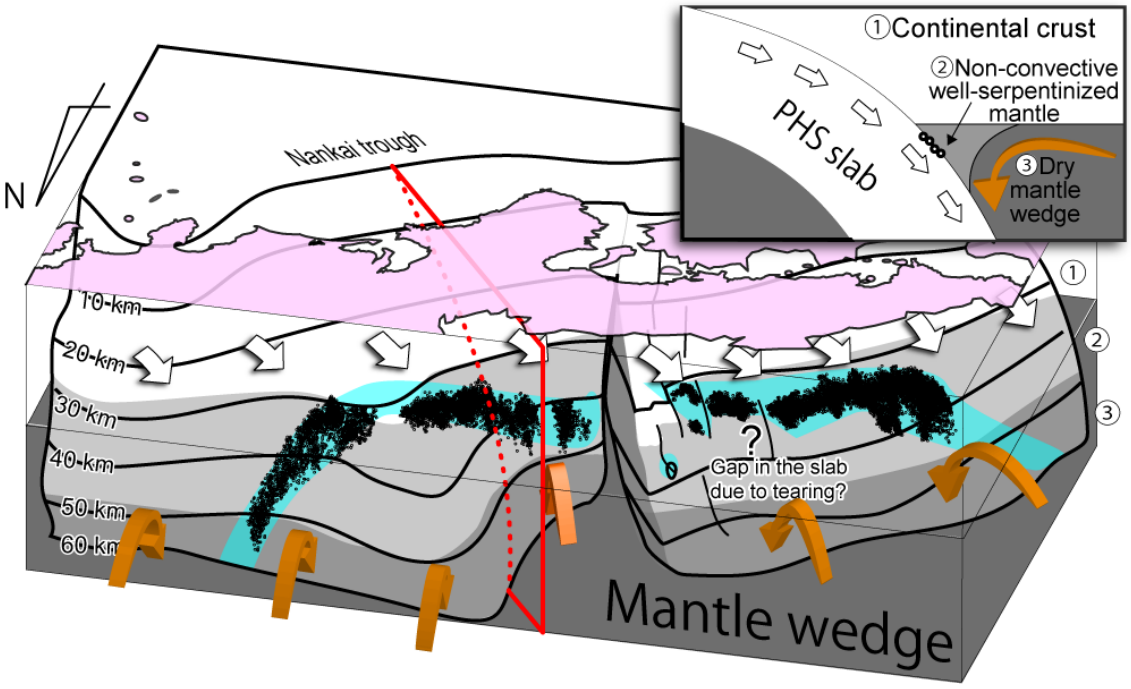

Figure 10. Schematic illustration showing slab motion (white arrows), torn and ruptured slab with isodepth contours, dehydration-derived fluid (blue), tremors (black circles). Hanging wall is divided by colors: From the top to bottom,

continental crust (white), non-convective well-serpentinized mantle (light gray), convective dry mantle (dark gray patch) with its convection by orange arrows.

1. Conclusion

Three-dimensional heat conduction and advection related to subduction of the PHS slab were simulated to compare the temperature of the slab with the along-dip location of the tremor belt. Starting from a semi-infinite flat cooled lithosphere for 15 Myr and progressing to subduction for 6 Myr, the tremor belt coincides with the ~450°C isotherm on the slab surface. This is the temperature at which the slab crust is transformed to eclogite via the dehydration of hydrous minerals. The dehydration-derived fluid results in serpentinization of the base of the mantle wedge, where the pressures and temperatures are within the stability field of serpentinite. The ~450°C isotherm is shallower within the tremor belt that outside the eastern and western margins of the belt, suggesting that tremor can occur only where dehydration-derived fluid encounters stagnant, well-serpentinized toe of the mantle wedge. The Ise and Kii gaps can be explained by the fact that the hanging wall is crust rather than mantle and that there is a step in the isotherm in the direction normal to plate convergence, respectively. An analysis of slab geometry indicates a tear in the deep extension of the slab beneath the Kii gap, which allows the step in the isotherm.

Acknowledgement

Yui Kobayashi is a student of the Future Scientists' School in Shizuoka University, a special program supported by Global Science Campus, Japan Science and Technology Agency. We thank Dr. Yoko Tu for her critical comments on the implications of the proposed cause of episodic tremor and slip. This work was also supported by JSPS KAKENHI Grant Number JP22H05302.

References

Annoura, S., Obara, K., & Maeda, T. (2016). Total energy of deep low-frequency tremor in the Nankai subduction zone, southwest Japan, *Geophysical Research Letters*, **43**, 2562-2567. doi:10.1002/2016GL067780.

Baba, T., Tanioka, T., Cummins, P. R., & Uhira, K (2002). The slip distribution of the 1946 Nankai earthquake estimated from tsunami inversion using a new plate model. *Phys. Earth Planet. Inter.* **132**, 59–73

Behr, W. M. , & Burgmann, R. (2021). What's down there? The structures, materials and environment of deep-seated slow slip and tremor. Phil. Trans. R. Soc. A 379: 20200218. doi: 10.1098/rsta.2020.0218.

Cummins, P. R., Baba, T., Kodaira, S., & Kaneda, Y. (2002). The 1946 Nankai earthquake and segmentation of the Nankai Trough, *Phys. Earth Planet. Inter.* **132**, 75-87

DeMets, C., Gordon, R., & Argus, D. (2010). Geologically current plate motions. *Geophys. J. Int.* **181** (1), 1–80, doi:10.1111/j.1365-246X.2009.04491.x

Evans, B. W. (2004). The serpentinite multisystem revisited: Chrysotile is metastable. *International Geology Review*, **46**:6, 479-506. doi:10.2747/0020-6814.46.6.479.

Hamaguchi, H., Goto, K. & Suzuki, Z. (1983). Double-planed structure of intermediate-depth seismic zone and thermal stress in the descending plate, *J. Phys. Earth,* **31,** 329–347. doi:10.4294/jpe1952.31.329

Hayes, G., 2018, Slab2 - A Comprehensive Subduction Zone Geometry Model: *U.S. Geological Survey data release*, doi:10.5066/F7PV6JNV.

Hirose, F., Nakajima, J. & Hasegawa, A. (2008), Three-dimensional seismic velocity structure and configuration of the Philippine Sea slab in southwestern Japan estimated by double-difference tomography, *J. Geophys. Res.*, **113**, B09315, doi:10.1029/2007JB005274

Hirose, H., Hirahara, K., Kimata, F., Fujii, N. & Miyazaki, S. (1999). A slow thrust slip event following the two 1996 Hyuganada earthquakes beneath the Bungo Channel, southwest Japan. *Geophys. Res. Lett.* **26**, 3237–3240.

Husker, A. L., Kostoglodov, V., Cruz-Atienza, V. M., Legrand, D., Shapiro, N. M., Payero, J. S., Campillo, M. & HuescaPérez, E. (2012). Temporal variations of non-volcanic tremor (NVT) locations in the Mexican subduction zone: Finding the NVT sweet spot, *Geochem. Geophys. Geosyst.*, **13**, Q03011, doi:10.1029/2011GC003916.

Ide, S., Beroza, G. C., Shelly, D. R., & Uchide, T. (2007). A scaling law for slow earthquakes. *Nature*, **447**, doi:10.1038/nature05780

Ide, S., Shiomi, K., Mochizuki, K., Tonegawa, T. & Kimura, G. (2010). Split Philippine Sea plate beneath Japan, *Geophys. Res. Lett.*, **37**, L21304, doi:10.1029/2010GL044585.

Ide, S. & Tanaka, Y. (2014). Controls on plate motion by oscillating tidal stress: Evidence from deep tremors in western Japan, *Geophys. Res. Lett.*, **41**, 3842–3850, doi:10.1002/2014GL060035.

Iidaka, T., Igarashi, T., Kato, A. & Iwasaki, T. (2017). Receiver function images of the distorted Philippine Sea slab contactwith the continental crust: Implications for generation of the 1891 Nobi earthquake (Mj 8.0). *Tectonophysics*, **717**, 41-50, doi:10.1016/j.tecto.2017.07.010

Isezaki, N. (1986). A magnetic anomaly map of the Japan Sea. *J. Geomag. Geoelectr.*, **38** (5), 403–410. doi:10.5636/jgg.38.403

Ji, Y., Yoshioka, S., & Banay, Y. A. (2017). Thermal state, slab metamorphism, and interface seismicity in the Cascadia subduction zone based on 3-D modeling. *Geophys. Res. Lett.*, 44, 9242–9252. doi:10.1002/2017GL074826

Julien, B. (2002). Seismological detection of slab metamorphism. *Science*, **296**, 1625-1626, doi: 10.1126/science.1072602

Kato, A. & Nakagawa, S. (2020). Detection of deep low-frequency earthquakes in the Nankai subduction zone over 11 years using a matched filter technique. *Earth, Planets and Space*, **72**: 128, doi:10.1186/s40623-020-01257-4.

Kimura, G., Hashimoto, Y., Kitamura, Y., Yamaguchi, A., & Koge, H. (2014). Middle Miocene swift migration of the TTT triple junction and rapid 4 crustal growth in SW Japan. *Tectonics*, **33**, 1219–1238. doi:10.1002/2014TC003531

Maruyama, S., Liou, J. G. & Terabayashi, M. (1996). Blueschists and Eclogites of the World and Their Exhumation. *International Geology Review*, **38**:6, 485-594. doi:10.1080/00206819709465347

Nakajima, J. & Hasegawa, A. (2007). Subduction of the Philippine Sea plate beneath southwestern Japan: Slab geometry and its relationship to arc magmatism. *J. Geophys. Res.*, **112**, B08306, doi:10.1029/2006JB004770.

Nakajima, J. & Hasegawa, A. (2016). Tremor activity inhibited by well-drained conditions above a megathrust. *Nat. Commun*, **7**, 13863, doi:10.1038/ncomms13863.

Obara, K. (2002). Nonvolcanic deep tremor associated with subduction in southwest Japan. *Science*, **296**, 1679–1681.

Obara, K. (2020). Characteristic activities of slow earthquakes in Japan. *Proc. Jpn. Acad., Ser. B*, **96**, 7, 297-315.

Okino, K., Shimakawa, Y. & Nagaoka, S. (1994). Evolution of the Shikoku Basin. *J. Geomag. Geoelectr.*, **46**, 463-479

Rogers, G. & Dragert, H. (2003). Episodic tremor and slip on the Cascadia subduction zone: The chatter of silent slip. *Science*, **300**, 1942–1943.

Salah, M. & Zhao, D. (2004). Mapping the crustal thickness in southwest Japan using Moho-reflected waves. *Phys. Earth planet. Int.*, **141** (2), 79-94. doi: 10.1016/j.pepi.2003.10.002

Shelly, D.R., Beroza, G.C., Ide, S. & Nakamula, S. (2006). Low-frequency earthquakes in Shikoku, Japan and their relationship to episodic tremor and slip. *Nature*, **442**, 188-191, doi:10.1038/nature04931.

Shiomi, K., Obara, K. & Sato, H. (2006). Moho depth variation beneath southwestern Japan revealed from velocity structure based on receiver function inversion. *Tectonophysics*, **420**, 205-221, doi:10.1016/j.tecto.2006.01.017

Shiomi, K., Matsubara, M., Ito, Y. & Obara, K. (2008). Simple relationship between seismic activity along Philippine Sea slab and geometry of oceanic Moho beneath southwest Japan. *Geophys. J. Int.*, **173**, 1018–1029, doi:10.1111/j.1365-246X.2008.03786.x.

Suenaga, N., Yoshioka, S., Matsumoto, T., Manea, V. C., Manea, M., & Ji, Y. (2019). Two-dimensional thermal modeling of the Philippine Sea plate subduction in central Japan: Implications for gap of low-frequency earthquakes and tectonic tremors. *J. Geophys. Res.*: Solid Earth, **124**, 6848–6865. doi:10.1029/2018JB017068

Takenaka, S., Sanshadokoro, H. & Yoshioka, S. (1999). Velocity anomalies and spatial distributions of physical properties in horizontally lying slabs beneath the Northwestern Pacific region. *Phys. Earth planet. Int.,* **112,** 137–157.

Wada, I. & Wang, K. (2009). Common depth of slab-mantle decoupling: Reconciling diversity and uniformity of subduction zones, *Geochem. Geophys. Geosyst.*, **10**, Q10009, doi:10.1029/2009GC002570.

Wada, I., Wang, K., He, J. & Hyndman, R. D. (2008). Weakening of the subduction interface and its effects on surface heat flow, slab dehydration, and mantle wedge serpentinization, *J. Geophys. Res.*, **113**, B04402, doi:10.1029/2007JB005190.

Wakita, H., Sano, Y., Mizoue, M. (1987). High ^{3}He emanation and seismic swarms observed in a nonvolcanic, forearc region. *J. Geophys. Res.* **92**, 12539–12546.

doi:10.1029/JB092iB12p12539

Yamaoka, K., Fukao, Y. & Kumazawa, M. (1986). Spherical shell tectonics: Effects of sphericity and inextensibility on the geometry of the descending lithosphere. *Rev. Geophys.*, **24** (1), 27-53.

Yoshida, A., Hosono, K., Takayama, H., Kobayashi, A. & Maeda, K. (2011). Seismic and geodetic evidence for the existence of hot materials beneath the Wakayama swarm activity, southwestern Japan. *Tectonophysics*, **510**, 124-131.

doi:10.1016/j.tecto.2011.06.023

Yoshioka, S., & Murakami, K. (2007). Temperature distribution of the upper surface of the subducted Philippine Sea Plate along the Nankai Trough, southwest Japan, from a three-dimensional subduction model: relation to large interplate and low-frequency earthquakes. *Geophys. J. Int.* **171**, 302-315. doi: 10.1111/j.1365-246X.2007.03510.x

Yoshioka, S., Toda, M., & Nakajima, J. (2008). Regionality of deep low-frequency earthquakes associated with subduction of the Philippine Sea plate along the Nankai Trough, southwest Japan. *Earth and Planet. Sci. Letters,* 272 (2008) 189–198. doi:10.1016/j.epsl.2008.04.039